PERGAMON

International Journal of Solids and Structures 40 (2003) 47–72

INTERNATIONAL JOURNAL OF SOLIDS and STRUCTURES

www.elsevier.com/locate/ijsolstr

Quantitative description and numerical simulation of random microstructures of composites and their effective elastic moduli

V.A. Buryachenko [a,*], N.J. Pagano [b], R.Y. Kim [a], J.E. Spowart [c]

[a] *University of Dayton Research Institute, 300 College Park, Dayton, OH 45433-0168, USA*
[b] *Air Force Research Laboratory, Materials and Manufacturing Directorate, AFRL/MLBC, Wright-Patterson AFB, OH 45433-7750, USA*
[c] *UES Incorporated, Dayton, OH 45433, USA*

Received 11 February 2002; received in revised form 25 July 2002

Abstract

A digital image processing technique is used for measurement of centroid coordinates of fibers with forthcoming estimation of statistical parameters and functions describing the stochastic structure of a real fiber composite. Comparative statistical analysis of the real and numerically simulated structure are performed. Accompanying of known methods of the generation of random configurations by the random shaking procedure allows creating of the most homogenized and mixed structures that do not depend on the initial protocol of particle generation. We consider a linearly elastic composite medium, which consists of a homogeneous matrix containing a statistically homogeneous set of ellipsoidal inclusions. The multiparticle effective field method (see for references, Buryachenko, Appl. Mech. Rev., (2001a), 54, 1–47) based on the theory of functions of random variables and Green's functions is used for demonstration of the dependence of effective elastic moduli of fiber composites on the radial distribution functions estimated from the real experimental data as well as from the ensembles generated by the method proposed.

Keywords: Microstructures; Inhomogeneous material; Elastic material

1. Introduction

The quantitative description of the microtopology of heterogeneous media, such as composite materials, porous and cracked solids, suspensions and amorphous materials, is crucial in the prediction of overall mechanical and physical properties of these materials. For example, many studies have shown that both tensile ductility and fracture properties of multy-phase composite materials are strongly affected by the spatial heterogeneity of the reinforcing phases. After many years of comprehensive study by direct measurements and empirical relations that is extremely laborious, the structure of microinhomogeneous

* Corresponding author. Fax: +1-937-656-7429.
E-mail address: buryach@aol.com (V.A. Buryachenko).

0020-7683/02/$ - see front matter © 2002 Elsevier Science Ltd. All rights reserved.
PII: S0020-7683(02)00462-6

materials are not completely understood. Computer simulation of topologically disordered structures by the random packing of hard spherical particles in 2D and 3D cases has a long history originated in the theory of liquids. This problem is closely connected with the known fundamental problem of statistical physics—description of the behavior of the particle system with interaction potential of hard spheres (see e.g. Binder and Heerman, 1997). Random packing of spheres has been studied very extensively due to their technological importance, and their opportunity to model the simple liquid, concentrated suspensions, amorphous and powders materials.

Computer simulation of packing problems can be classified into three groups of methods: molecular dynamic, Monte Carlo, and dense random packing. Much progress in the theory of the dense random packing was approached by the use of two kinds of methods: the sequential generation models and the collective rearrangement models (CRM). In the sequential model by Bennet (1972), so called cluster growth model, a particle being added to the surface of particle cluster which grows outwards is placed sequentially to the point closest to the original such that the new particle established contact with three existing spheres in the cluster. Overlapping is ruled out by checking the center–center distance of the particle. This algorithm was modified (see Lu et al., 1994) by including an artificial input parameter, "coefficient of tetrahedron perfection", k^{tp} to require that a triangular site would be filled only if the resulting tetrahedron satisfied a minimum k^{tp} requirement which ranged from requiring perfect tetrahedra, $k^{\mathrm{tp}} = 1.0$, to placing no requirement on triangular sites except that the added sphere would touch all three of the spheres which made up the site, $k^{\mathrm{tp}} = 2.0$. Phenomenological character of the construction algorithm posed the particle cluster from the initial term containing three particles leads to the inhomogeneous and anisotropic inclusions fields with the different density that was demonstrated by Boudreaux and Gregor (1977). Moreover, the configurations generated do not demonstrate the characteristic split second peak in the radial distribution function (RDF) observed in experimental packing. Kansal et al. (2000) proposed algorithm controlling the degree of order throughout the formation of the packing of growing clusters. In the second type of sequential generation model, called the model of "rigid sphere free fall into a virtual box", one particle is dropped vertically each time from the random point onto the surface of an existing particle cluster growing upwards (see e.g. Nolan and Kavanagh, 1992; Cesarano et al., 1995; Kondrachuk et al., 1997; Furukawa et al., 2000). The different densities were approached by introducing a phenomenological parameter limiting the number of rotations of each fallen sphere until it becomes a permanent part of the structure. Effects of boundaries of the virtual box are eliminated by introducing conventional cyclic boundary conditions. The algorithms described belong to the class of static methods where the particles are placed at a given time step and cannot thereafter move. For contrast, dynamic methods assume the reorganization of whole packing due to either short or long range interactions between particles. In the CRM, N-points randomly distributed in a virtual box are assigned both radii and random motion vectors. Each sphere is moved until there are no overlaps. Then the radii are increased and the process is repeated until any further increase in radii or any displacement of the spheres create overlaps that can not be eliminated (the different versions of this method can be found e.g. in Clarke and Willey, 1987; Lubachevsky and Stillinger, 1990; Lubachevsky et al., 1991; Zinchenko, 1994; Knott et al., 2001; He and Ekere, 2001; see also Ogen et al., 1998 where a detailed description of the advantages and drawbacks of the different algorithms were presented). More recently, numerical simulations were performed to realize homogeneous and isotropic packing of spheres by various methods, for instance, by assuming hypothetical spheres having dual structure whose inner diameter defines the true density and the outer one a nominal density (see Jodrey and Tory, 1985). An alternative approach (eliminating the boundary effect of the virtual box) is based on the use of spherical boundary conditions instead of periodic ones (see e.g. Hall, 1988; Tobochnik and Chapin, 1988). There one simulates hard disks (more exactly a circular cap which can be visualized as a contact lens on the surface of an eyeball) on the surface of the ordinary three-dimensional sphere and hard spheres on the "surface" of a four-dimensional hyposphere. The advantage of this procedure is that there is no preferential direction, and it is impossible to pack particles into perfect regular periodic configurations.

Close random ensembles of spheres have been studied for many years, and the following quantitative parameters are well-known. Packing densities for close lattice packing are $\pi/\sqrt{12} \approx 0.9069$ (triangular) in the case of disks packing into the plane, and $\pi/\sqrt{18} \approx 0.7405$ (fcc or hcp) in the case of spheres packed into R^3. Model experiments were performed using steel balls of equal size randomly packed into shaking containers. The measured densities are extrapolated to eliminate finite-size effects. These models provide the conventional value of random close packing such as $c^{\mathrm{RCP}} = 0.6366 \pm 0.004$. Random loose packing equal $c^{\mathrm{RLP}} = 0.60 \pm 0.2$ is observed at the gentle rolling of a steel balls into the packing container without shaking. In two dimensions, the experimental numbers for close and loose random packing are estimated with less accuracy $c^{\mathrm{RCP}} = 0.8225$ and $c^{\mathrm{RLP}} = 0.601$. (see for references Berryman, 1983; Cheng et al., 2000). It should be mentioned that in contradistinction to the periodic packing, a random close packing is ill defined problem which has no unique theoretical definition and its final states are protocol dependent in both the numerical simulation and experimental sense (see for details Torquato et al., 2000).

Since the overall properties of fiber composite materials are sensitive to the details of the microstructure, the geometrical basis for modeling actual microstructures is needed. Digital image analysis is available for estimation of descriptors of the spatial arrangement of microstructural features observed in a transverse cross-section of the material based on the *stereological* technique (see e.g. Berryman, 1985; Stoyan, 2000). The classical stereology investigates the spatial structures by planar sections, and statistically analyzes the visible structures. For example, the local stereology (see Jensen, 1998) shows how mean particle volumes can be estimated by length measurement. In general, some important spatial characteristics cannot be estimated stereologically, and the statistical methods based on new microscopic techniques (e.g. confocal microscopy, see König et al., 1991; Karlsson and Liljeborg, 1994) using three-dimensional measurement were proposed. For example, by moving the local plane of a confocal scanning laser microscope up or down through the specimen, a stack of serial sections, called a brick, is obtained, from which a 3D image may be produced without the need to use physical sections.

Space Dirichlet tessellations subdividing an Euclidian space into n-dimensional bounded convex polytopes (polygons in 2D case) are widely used to characterize the spatial distribution, size, and shape of a filled phase (see e.g. Ghosh and Mukhopadhyay, 1991). They provide a natural and unique approach for defining a particle's neighbors and neighborhood. The Dirichlet tessellation of two-dimensional domain w yields a network of convex Voronoi polygons containing one inclusion with the center $\mathbf{x}_i$ ($i = 1, \ldots, n$) each, at most. The interior of Voronoi cell associated with the point $\mathbf{x}_i$ is the region $w_i = \{\mathbf{x} \in w : |\mathbf{x} - \mathbf{x}_i| < |\mathbf{x} - \mathbf{x}_j|,\ \forall j \neq i\}$ that is the neighborhood of $\mathbf{x}_i$. The tessellation is constructed by plotting lines to the centers of all nearby particles and then constructing perpendicular bisecting planes to those lines. Green and Sibson (1977) have proposed the algorithm generating Voronoi polygons for n-points by computing in $O(n \log n)$ time by tracing boundary adjustment, as a new polygon is fitted into a previously generated set. Ghosh and coworkers (see for references Ghosh et al., 1997) have developed a material based Voronoi cell method for directly treating multiple phase Voronoi polygons as elements in a finite element model for elastic and termoelastoplastic problems; they suggested a modification to the standard tessellation procedure to preclude the situation where neighboring fibers are substantially different in size and are closely spaced, that may result in polygons which do not completely envelope their corresponding fibers, and may instead "cut" through the fibers. Since each Voronoi cell contains a single particle surrounded by the matrix, the Dirichlet tessellation can be used for description of a statistical structure of composites in the form of the frequency distribution, for all cells, of the ratio in particle-to-cell volume that is also a measure of particle clustering in microstructure (see e.g. Bhattacharyya and Lagoudas, 2000).

In Section 2 of the present paper, the quantitative descriptors of the dispersion of fibers in unidirectional composites will be analyzed in order to describe the pattern of fiber location as it really exists rather than as described by some assumed model. Since random packing structures are strongly dependent on the procedure of their generation, in Section 3 we will consider a few popular algorithms and their combinations adapted for obtaining the most homogeneous configurations, and will compare the statistical parameters of

configurations generated by the different methods. In Section 4 one will estimate the dependence of effective elastic properties of fiber composites on the RDF estimated from the real experimental data as well as from the ensembles generated by each proposed method.

2. Statistical description of random structure composites

2.1. Some background notions and definitions

Let a linear elastic infinite body occupying full space R^d contains an open bounded domain $w \subset R^d$ (window of observation) with a boundary Γ and with a characteristic function W and space dimensionality d ($d = 2$ and $d = 3$ for 2D and 3D problems, respectively). The domain w contains a homogeneous matrix $v^{(0)}$ and a random finite set $X = v_i$ $(i = 1, \dots, N(w))$ of inclusions v_i with centers $\mathbf{x}_i$ and with characteristic functions $V_i(\mathbf{y})$ equals one in $\mathbf{y} \in v_i$ and zero otherwise and bounded by the spherical surfaces $\Gamma_i = \{\mathbf{y} : |\mathbf{y} - \mathbf{x}_i| = a\}$; $v^{(1)} = \cup v_i$ $(i = 1, 2, \dots, N)$. $N = N(w)$ denotes the random number of points $\mathbf{x}_i$ falling in w; $\widehat{N}(w)$ is the observed number of points in w.

At first we summarized some basic ideas, notations and quantities for random point processes such as e.g. centers of particles (for more details the reader is referred to Ripley, 1977, 1981; Diggle, 1983; König et al., 1991; Stoyan and Stoyan, 1994; Stoyan, 2000; Torquato, 2002). We will consider statistically homogeneous (or stationar) and isotropic ergodic random field X, keeping in mind that the stationarity, isotropy, and ergodicity can never be tested statistically in their full generality. Stationarity means invariance under arbitrary translation, and isotropy means invariant under arbitrary rotation. The ergodicity ensured that one sample (one-point pattern) is sufficient for obtaining statistically secure results, assuming the convergence of results obtained for infinitely expanding observation window w. The intensity, $n = EX([0,1]^d)$, of a stationary point process is the mean number of points in the unit cube. A common unbiased estimator is $\hat{n} = N(w)/\bar{w}$, $\bar{w} \equiv \operatorname{mes} w$.

The packed random structure can be characterized by several parameters, such as packing density, coordination number, RDF, particle cage, inter-particle spacing, and others. The various methods of estimating the effective properties of a composite material use a knowledge of statistical geometrical information about the microstructure. In order to incorporate the spatial arrangement of components in a micromechanical simulation, it is essential to quantitatively characterize the random structure of the composite. The most important factors characterizing the microstructure of composite material are the shape, volume fraction, and arrangement (random or regular) of the components that permit the calculation of bounds of effective moduli. The popular statistical description of microinhomogeneous media is based on expectations of products of the characteristic function $V^{(i)}(\mathbf{y})$, assuming that the role of the matrix is assigned to phase '0'. In a simple case the bounding of effective properties uses the multipoint statistic reducing to only one-point probability density (volume fraction) $S_1^{(i)}(\mathbf{y}_1)$ defined as

$$S_1^{(i)}(\mathbf{y}_1) = \langle V_i(\mathbf{y}_1) \rangle, \tag{2.1}$$

where the angle brackets $\langle(\cdot)\rangle$ denote an ensemble average. Improved bounds on a variety of different effective properties have been derived in terms of n-point probability density

$$S_N^{(i)}(\mathbf{y}^N) = \langle V_i(\mathbf{y}_1), \dots, V_i(\mathbf{y}_N) \rangle, \tag{2.2}$$

i.e. the probability of simultaneously finding of n-points in a specified geometrical arrangement $\mathbf{y}^N \equiv \mathbf{y}_1, \dots, \mathbf{y}_N$ in one of the phases. For example, the one-point correlation function is the probability that any point lies in any particular. The two-point probability function is the probability that both two-points $\mathbf{y}_1$ and $\mathbf{y}_2$ lie in the same phase. This function provides a method for experimentally determining the low-

order multipoint moments for real two-phase media, as considered by Corson (1974). The medium is assumed to be statistically homogeneous, i.e. $S_N^{(i)}(\mathbf{y}^N)$ is translationary invariant for any $\mathbf{y} = \text{const}$.

$$S_N^{(i)}(\mathbf{y}^N) = S_N^{(i)}(\mathbf{y}_1 + \mathbf{y}, \ldots, \mathbf{y}_N + \mathbf{y}). \tag{2.3}$$

Statistical isotropy of the medium being assumed means invariant under arbitrary rotation. It is also known that the conventional bounds on effective properties are given in terms of other types of statistical quantities such as point/q-particle functions, surface–surface correlation functions, nearest neighbor distribution (NND) function, linear-path function, two-point cluster function, chord-length distribution function as well as the generalized n-point distribution function for the system of identical spheres $H_n(\mathbf{y}^m; \mathbf{y}^{p-m}; \mathbf{r}^q)$, which is defined to be the correlation associated with finding m points with positions $\mathbf{y}^m$ on certain surface within the medium, $p - m$ with positions $\mathbf{y}^{p-m}$ in certain space exterior to the spheres, and q sphere centers with positions $\mathbf{r}^q$, $n = p + q$ (see for details Torquato, 2002 and references therein). However, although higher-order correlation functions ($N > 3$) are obtained on theoretical grounds, this is not a very practicable approach.

Usually the statistical description of the microstructure is performed in terms of the characteristic functions $V_i(\mathbf{y})$. An alternative related approach of quantitative description of the composite microstructure is based on the consideration of the inclusion centers statistically described by the multiparticle probability densities $f_m(\mathbf{x}_1, \ldots, \mathbf{x}_m)$ that give the probability $f_m(\mathbf{x}_1, \ldots, \mathbf{x}_m)\,\mathrm{d}\mathbf{x}_1, \ldots, \mathrm{d}\mathbf{x}_m$ to find a sphere center in the vicinities $\mathrm{d}\mathbf{x}_1, \ldots, \mathrm{d}\mathbf{x}_m$ of the point $\mathbf{x}^m = (\mathbf{x}_1, \ldots, \mathbf{x}_m)$. The f_m are the most basic descriptors that characterize the structure of many-particle system and have been well-studied in the statistical mechanics of liquids (Hansen and McDonald, 1986). In particular, $f_1 = n$, where n is the number density of inclusions connected with the volume fraction $c = n\bar{v}_i$, $\bar{v}_i \equiv \operatorname{mes} v_i$. The widely used two-point density $f_2(r) = f_2(\mathbf{x}_1, \mathbf{x}_2)$ ($r = |\mathbf{x}_1 - \mathbf{x}_2|$) is expressed in terms of RDF $g(r)$ as

$$f_2(r) = n^2 g(r). \tag{2.4}$$

In the framework of the simplest "two-point" level, Markov and Willis (1998) demonstrated a simple interconnection expressing $S_2^{(1)}(\mathbf{y}^2)$ as a simple one-tuple integral containing the RDF $g(r)$ (2.4). Torquato and Stell (1985) have related $S_N^{(1)}$ to multidimensional integrals over the infinite set of m-particle densities $f_1, \ldots, f_m$ ($m \to \infty$).

The widely used informative function which describes the point distribution is the *second-order intensity function* $K(r)$ (called also Ripley's K function) defined as the number of further points expected to be located within a distance r of an arbitrary point divided by the number of points per unit area n. Since points lying outside the observation window w are non-observed, the latter depends strongly on the shape and the size of w. It is our aim to simulate typical realization which also includes interaction to the structure element outside of the window while avoiding systematic errors or biases in the estimation procedure. The effect of the edge of the domain w becomes increasingly dominant at the dimensional increases. A number of special edge corrections are known. A naive way proposed in *the minus-sampling* method is to consider w^* within domain w and allow measurements from an object in w^* to an object in w. Although the effective sample size is then the number of points in w, the method, of course, leads to a big loss of information. A much better idea of edge-correction of the estimator for $K(r)$ was suggested by Ripley (1977)

$$\widehat{K}(r) = \frac{\bar{w}}{\widehat{N}^2} \sum \sum_{i \neq j} w_{ij}^{-1} I_{ij}(r_{ij}), \tag{2.5}$$

where $\widehat{N}$ is the number of points $\mathbf{x}_k$ ($k = 1, \ldots, \widehat{N}$) in the field of observation w with the area $\bar{w}$, $I_{ij}(r_{ij})$ is the indicator function equals 1 if $r_{ij} \leqslant r$ and zero otherwise where r_{ij} is a distance between the points $\mathbf{x}_i$ and $\mathbf{x}_j$. w_{ij} is the ratio of the circumference contained within w to the whole circumference with radius r_{ij}. For circles intersecting the boundary ∂w, the function w_{ij} compensating for the boundedness of w is less than

one and has an explicit formula when the field of observation w is rectangular (see Diggle, 1983; the formulae and algorithm for 3D case were proposed by König et al., 1991). The function $K(r)$ (2.5) is obtained by averaging over all inclusions at each value of r. Eq. (2.5) is an approximately unbiased estimator, which is free of systematic errors, for sufficiently small r because $N/\bar{w}$ is a slightly biased estimator for n. In 2D, Diggle (1983) recommended an upper limit of r equal to half the length of the diagonal of a square sampling region.

Due to the wide utilization of periodic boundary conditions in numerical simulations of random packing, an alternative *toroidal edge correction* is often used (and precisely this method will be explored hereafter in this paper for the elimination of the boundary effect) in which each rectangular region w can be regarded as a torus, so that points on opposite edges are considered to be closed. Then w can be considered to be part of a grid of identical rectangles, forming a border around the pattern inside w. Distances are then measured from the point in the central rectangle w to points in the surrounding periodic rectangles (see Ripley, 1981).

The RDF $g(r)$ (2.4) which plays a role similar to the variance in a classical analysis of random variables is defined as the radial distribution of the average number of sphere centers per unit area in a spherical shell. The RDF can be estimated from second-order intensity function as

$$g(r) = \frac{1}{d\omega_d r^d} \frac{\mathrm{d}K(r)}{\mathrm{d}r}, \tag{2.6}$$

where ω_d is the volume of the unit sphere in R^d. The RDF is related to the derivative of $K(r)$ (2.6), and is therefore it is more sensitive to changes in the spatial order than is the function $K(r)$.

The interaction effects generating the local stresses produced by inclusions are highly sensitive to their locations. In so doing the non-linear processes such as fracture and fatigue are far more sensitive to local stresses and, therefore, to local variations of microstructure then other mechanical phenomena. Because of this, in the deformation and fracture processes,another important statistical parameter of the location of inclusions is a NND function (see e.g. Pyrz, 1994) defined by the density $N^{\mathrm{nd}}(r)$ such that $N^{\mathrm{nd}}(r)\,\mathrm{d}r$ equals to the probability that there is no other inclusion centroid in a circle of radius r with the center $\mathbf{x}_i$, and there is at least one inclusion centroid in the ring of radius r and $(r + \mathrm{d}r)$. Ripley (1977) introduced the following unbiased estimator for $N^{\mathrm{nd}}(r)$ taking the edge effect into account. For $\mathbf{x}_1, \ldots, \mathbf{x}_N \in w$, let ρ_i be the distance from the point $\mathbf{x}_i$ to its nearest neighbor in w, and let ρ_i^{∂} be the shortest distance from $\mathbf{x}_i$ to the boundary ∂w. Then the estimator for $N^{\mathrm{nd}}(r)$ is given by

$$N^{\mathrm{nd}}(r) = \frac{\#\{\rho_i \leqslant r \wedge \rho_i^{\partial} > r\}}{\#\{\rho_i^{\partial} > r\}}, \tag{2.7}$$

where $\#(\cdot)$ is the counting function which tallies the number of points in the specified set. In the estimator (2.7), only the points are analyzed for which the nearest neighbor distance ρ_i is smaller than the smallest distance ρ_i^{∂} to the boundary ∂w. The average neighbor distance $\langle N^{\mathrm{nd}} \rangle$ is found by the formula

$$\langle N^{\mathrm{nd}} \rangle = \int_0^{\infty} r N^{\mathrm{nd}}(r)\,\mathrm{d}r. \tag{2.8}$$

The nearest neighbor and higher-order neighbor distributions can be estimated experimentally by measuring the frequency of occurrence of different distances of different order neighbors of the inclusions for a large number of inclusions.

2.2. Materials and image analysis procedures

A carbon fiber-reinforced epoxy composite is chosen for microstructural analysis. Ten specimens of this composites produced by the different technological regime are analyzed. Each specimen containing 10

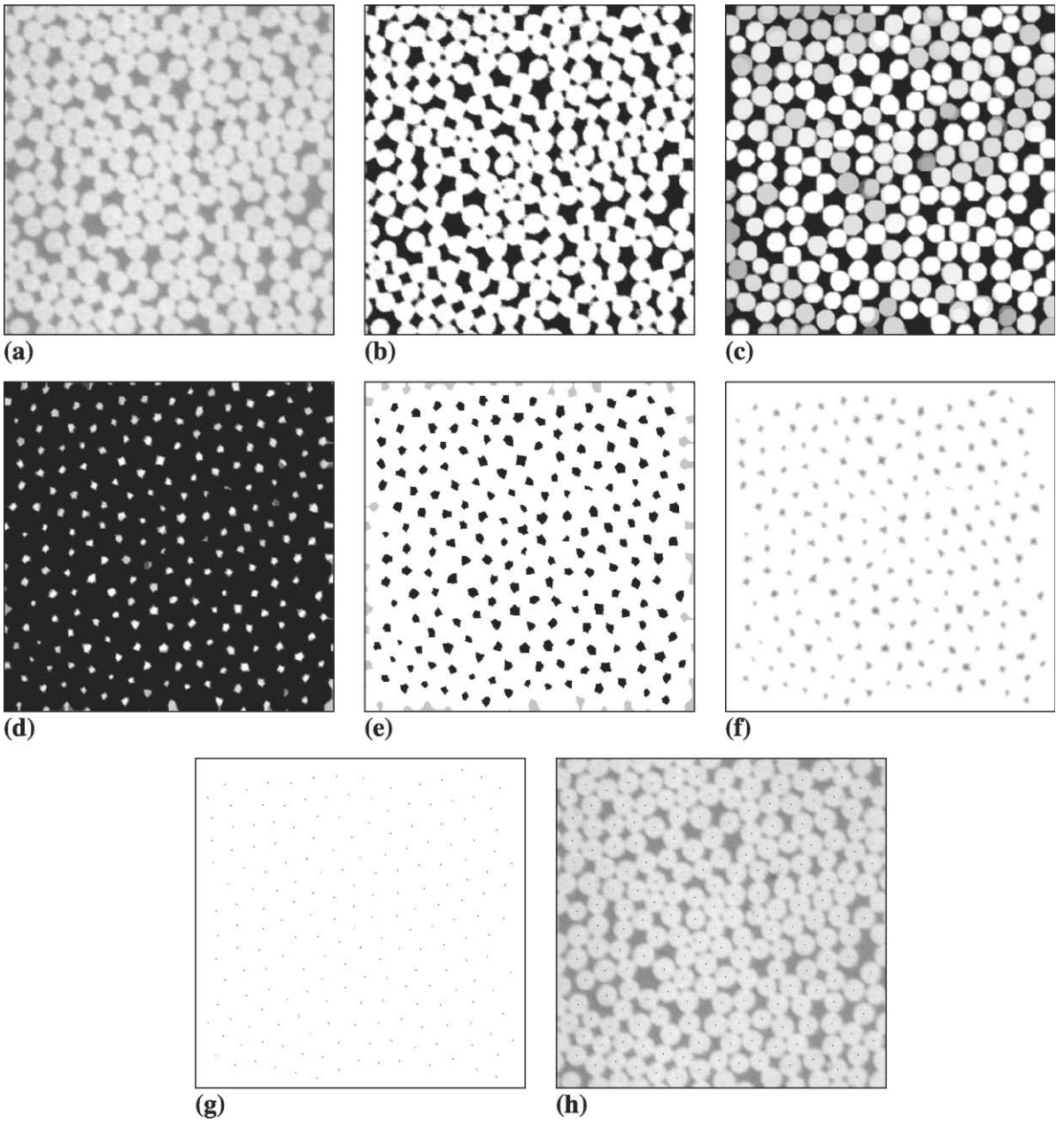

Fig. 1. (a) Fragment of the original micrograph of fiber composite material microstructure; (b) unsharp mask applied; (c) closing operation applied; (d) darkest filter applied; (e) thresholded image (gray edge features are rejected); (f) EDM applied; (g) fiber centroids; (h) combined image showing centroid positions on original fiber profiles.

samples was cut using a diamond saw from a unidirectional composite laminate, and each specimen was first sanded and then polished to a 0.5 μm finish on the cross-section area, 20 mm × 1.5 mm. A microscopic image with 200× magnitude for microstructural analysis of samples was taken using an optical microscope.

Each image of the sample contains approximately 1800 fibers. The fiber volume and spatial distribution were determined from the image analyzer that is capable of calculating the fiber volume and the coordinate of each fiber.

Digital images of transverse sections through the fiber composite material were obtained by digitizing high-resolution optical micrographs, using standard methods (see e.g. Louis and Gokhale, 1994; Spowart et al., 2001; Shan and Gokhale, 2002 where additional references can be found). Care was taken to maximize the contrast between the fibers and matrix in the original micrograph, Fig. 1(a). Image processing was then carried out on the 1024×1024 digital images using a commercially-available desktop software package (Adobe Photoshop 5.5) in conjunction with a plug-in Image Processing Tool Kit (see Russ, 2001). The following sequence of operations was applied to the grayscale digital images in order to locate the fiber centroids in the transverse plane.

First, an Unsharp Mask is applied, Fig. 1(b). This filter increases the contrast between the fibers and the matrix, and assigns the central portion of each fiber a uniform gray level. This reduces the influence of fiber edge effects, allowing a more accurate determination of the true fiber centroid. To be most effective, the mask is applied at the highest level (500%), over a distance roughly equivalent to the mean fiber diameter.

Next, a closing (rank) operation is carried out on the image to separate each fiber from its neighbor, Fig. 1(c). The rank operation is applied to every pixel in the image, and extends over a 3×3 pixel neighborhood, equivalent to 5% of the mean fiber diameter. After the filter has been applied, neighboring fiber profiles are effectively segmented by assigning them different grayscale values. The separation of each fiber by grayscale in this manner allows each fiber profile to be recognized as a distinct microstructural feature, which is crucial to the determination and assignment of individual fiber centroid coordinates.

The Darkest (rank) filter is then applied to every pixel in the image, Fig. 1(d). This operation automatically selects the darkest pixel in the 3×3 neighborhood surrounding the central pixel, and replaces the central pixel with this grayscale value. The darker areas in the image (corresponding to the matrix areas between the individual fibers) therefore propagate outwards, effectively reducing the extent of the fiber features until only their cores remain. The image is then thresholded to obtain a binary image, and then inverted to produce black fiber features on a white matrix background, Fig. 1(e). Fiber profiles that intersect the edges of the image are rejected in subsequent processing steps.

A Euclidean distance map (EDM) filter is then applied to the image, Fig. 1(f). This filter assigns grayscale values to the pixels within each fiber feature, according to their linear distance from the edge of the feature. Thus, the pixels at the centroids of each fiber are assigned the highest gray levels. An additional binary erosion step is sometime needed here, if the EDM operation does not result in a single pixel at the centroid of each fiber the first time. This has only a minor effect on the overall results. Finally, the image is thresholded again, to produce an image with single black pixels at each of the fiber centroids, Fig. 1(g).

Once the image is reduced to an array of black pixels corresponding to the centroid positions of each fiber profile, it is a simple matter to extract the coordinates, using the IPTK software or any other suitable computer code. The coordinates are output as integer pairs in the range [1,1024], and are subsequently renormalized for input into the microstructural models.

3. Numerical simulation

Since random packed structures are strongly dependent on the procedure of their generation, we will consider a few popular algorithms and their combinations, and will compare the statistical parameters of configurations generated by each different method.

3.1. Poisson distribution

Various models have been proposed for the generation of center coordinates of randomly packed spheres. If the sphere radii are small enough then their centroid coordinates will be described by the stationary (or homogeneous) Poisson point process for which: for any bounded region w the number of points of X falling in w follows the Poisson distribution

$$P(N(w)=k)=\frac{(n\bar{w})^k}{k!}\exp(-n\bar{w}),\quad k=0,1,\dots \tag{3.1}$$

and for non-overlapping sets $w_1,\dots,w_m$, the numbers $N(w_1),\dots,N(w_m)$ are independent random variables. These properties imply stationarity and isotropy because of the translation and rotation invariance of volume. A further implication is that the point positions are independent and uniformly distributed within w. The uniform (binomial) point process of a given number $N(w)=N$ of points $\mathbf{x}_1,\dots,\mathbf{x}_N$, independent and uniformly distributed in w, if for non-overlapping bounded $w_1,\dots,w_N\subset w$,

$$P(\mathbf{x}_1\in w_1,\dots,\mathbf{x}_N\in w_N)=(\bar{w}_1,\dots,\bar{w}_N)/(\bar{w})^N \tag{3.2}$$

with the binomial distribution of the number of points in any bounded region $w_j\subset w$:

$$P(N(w_j)=k)=\binom{N}{k}^k(p(w_j))^k(1-p(w_j))^{N-k},\quad k=0,1,\dots,N, \tag{3.3}$$

where $p(w_j)=\bar{w}_j/\bar{w}$, $EN(w_j)=Np(w_j)$ and $\mathrm{Var}N(w_j)=Np(w_j)(1-p(w_j))$.

A stationary Poisson point process may serve as a reference model for complete spatial randomness and can be easily simulated with a computer. For example, $N(w)$ points are generated with uniform random position in a region $w=[0,L_1]\times\cdots\times[0,L_d]$ as a sequence of $dN(w)$ independent random numbers $x_1,\dots,x_{dN(w)}$ uniformly distributed on $[0,1]$ and generated by a random number generator. The coordinates of the ith $(i=1,N(w))$ point are then $\mathbf{x}_i=(L_1x_{di-d+1},\dots,L_dx_{di})^\top$. Although the hypothesis of a Poisson set of centers for non-overlapping spheres is not fulfilled for finite sphere radii, it can often be used as a useful approximate description of the observed structures (see Ripley, 1977).

We recall that for Poisson distribution

$$K(r)=\omega_d r^d,\quad \text{and } g(r)=1, \tag{3.4}$$

and the expectation mean $\langle N^{\mathrm{nd}}\rangle$ and variation $E(s^2)$ of nearest neighbor distances are estimated as ($d=2$, see Spitzig et al., 1985)

$$\langle N^{\mathrm{nd}}\rangle=0.4n^{-1/2},E(s^2)=\frac{4-\pi}{2\pi n}. \tag{3.5}$$

3.2. Hard core model

The extension of Poisson distribution process as a static model is the generation of random assemblies of n non-overlapping disks by the hard core model (HCM) (called also random sequential adsorption model, see e.g. Feder, 1980; Hinrichsen et al., 1986 and simple sequential inhibition): disks with radius a are placed one by one with the center positions $X=(\mathbf{x}_1,\dots,\mathbf{x}_N)$ being distributed randomly and uniformly over the set of all points in a rectangular region ω of size $[-0.5,0.5]\times[-0.5,0.5]$. Although the distribution of disks depends heavily on the shape and size of w, usually researchers assume in mind a homogeneous structure in the whole space which is observed only in w. To avoid this discrepancy, one supposes the periodic boundary conditions, that is ω and X are periodically replicated in all directions. If the new disk does not overlap already deposited disks, its position is fixed and does not move anymore; otherwise, it is rejected and

another random center position is generated. The process is finished when either a preassigned packing fraction is achieved or when no more particles can be added (jamming limit) which occurs at a volume fraction $c \approx 0.55$ (2D case) or $c = 0.38$ (3D case) (see Tanemura, 1979; Lotwick, 1982). The mathematically formalized descriptions of other versions of the HCM using either a technique of a birth-and-death process with vanishing death rate or the Matern's thinning rule can be found in Stoyan et al. (1995).

The HCM provides a more realistic reference model than a Poisson point process, in which arbitrary small distances between points are allowed. The advantage of protocol independence in the HCM is sacrificed in the case of generation of binary or polydisperse structures (see e.g. Davis and Carter, 1989; Sinelnikov et al., 1997; He et al., 1999). Indeed, after an unaccepted trial one can keep the previous choice of inclusion radius or choose to replace it. The real situation then lies between two limiting cases of jamming limits, the packing density generated by first placing the larger particles and then the smaller particles will be higher than the opposite case, where the small particles are placed before the big ones. The geometrical blocking effect and the process irreversibility leads to packing configurations that are essentially different from the corresponding equilibrium configuration (see Widom, 1966). To prevent just this kind of low-density jamming in the following model, we will shake the disks.

3.3. Hard core shaking model

Hard core shaking model (HCSM) is a type of HCM which generates an increasing number of inclusions in a virtual box w accompanied by a shaking process, i.e. giving each disk a small random displacement independent of its neighbors' positions. This makes it possible to unlock the disks from the jamming configuration (which takes place for HCM at $c \approx 0.55$) and allows them to find the most homogeneous and mixed arrangement. Various algorithms have been devised to simulate reordering due to shaking or vibration of dense packing (see Barker, 1993) which reduces the volume concentration of the high density jam configuration. Packing configurations containing a wide range of inclusion concentrations have been investigated less and necessitative some additional consideration. In order to describe the algorithm used in this paper, at first one introduces the following definitions.

To speed up the calculations it is useful to check the collision partners $v_j (j = j_1^i, \ldots, j_{n_t}^i)$ of v_i only in some restricted neighborhood of $\mathbf{x}_i$ called testing window $w_t^i = \{\mathbf{x} : |\mathbf{x} - \mathbf{x}_i| < R_t\}$ ($R_t = \text{const.}$). In this model, the neighbors of a disc are considered to be the set of discs whose centers lie within some maximum distance called the testing window w_t^i of that disk rather than the "geometric neighbors" which can be determined by the more computationally expensive Delaunay tessellation (see e.g. Okabe et al., 1992). The reason for the use of the testing window w_t^i instead of the Delaunay tessellation is that each $n_t \bar{v}_i$ is an estimation of local volume fraction which coincides with c only for an infinitely large testing window. If $n_t < 7$ for $R_t = 3a$ then a new uniformly distributed inclusion is generated in the area $w_t^i \setminus v_i^0$ in a spirit of the HCM described above, where v_i^0 is a spherical "included volume" with the center $\mathbf{x}_i$ and the radius $2a$ (since inclusions cannot overlap).

Another way to speed up the calculations is to carry out the shaking process only within a local shake up window. The random local shaking is established in a shake up window $w_{\text{sh}} = \{\mathbf{x} : |\mathbf{x} - \mathbf{x}_i| < R_t - 2a\}$ ($R_t = \text{const.}$) whereby the inclusion center $\mathbf{x}_i$ is randomly moved to a position $\mathbf{x}_i'$ uniformly distributed in w_{sh}. If the particle does not overlap with any other inclusions the shaking is accepted, otherwise the trial shaking is repeated until the number of attempted trial shakings exceeds some limit. Only the near neighbor set of inclusions v_j $(j = j_1^i, \ldots, j_{n_t}^i)$ which are located in the testing window w_t^i are checked for overlap, which also reduces the computer time. One determines the optimal size for the shake up window $R_t - 2a = 1.1a$ which provides the minimum average number of trial shaking attempts. This number increases from 5 to 8 when the packing density grows from $c = 0.5$ to 0.8. This size of shake up window provides the fastest stabilization of statistical parameter estimations. However, their values do not depend on the size of the window and are, furthermore, protocol independent (in contrast with the known methods

of random close packing simulations, see e.g. Torquato et al., 2000). The shaking process passes through all inclusion (so called global shaking) with re-estimation of the neighbor inclusions in the testing window w_t^i after each local shaking of the inclusion v_i. In so doing, the increasing number of shaking has a twofold effect. On the one hand, the system is becomes more homogeneous and well-mixed and on the other hand, the stochastic fluctuations of statistical parameters (such as e.g. $g(r)$ and $N^{\rm nd}(r)$) estimated by averaging of these structures tend to diminish.

In Fig. 2 comparative analyzes of the RDF $g(r)$ as a function of r estimated by the HCM and HCSM are presented for the fiber concentrations $c = 0.5$, 0.55. The plot of $g(r)$ of the configuration generated by the HCM was obtained by the averaging over 30 realizations; the other curves each correspond to a single realization. In so doing, the regular shaking procedure of the HCSM yields the fitting of averaging curves $g(r) \sim r$. As can be seen, the HCSM leads to more long range ordering than the HCM, and at the same c the RDF $g(r)$ for a small r is higher for structures simulated by the HCM rather than by the HCSM. It should be mentioned that for a population of finite size fibers, a value of $g(r)$ higher than 1 does not necessarily imply that the fibers are clustered. Comparison of the histograms of the average number n_t of inclusions in the rectangular testing window $w_t^i = \{\mathbf{x} : |x_l - x_{il}| < R_t, l = 1, 2\}$ ($R_t = 3a$) is presented in Fig. 3 from the figure we notice that the compromise of the shaking procedure with the modified HCM leads to a more homogeneous and well-mixed arrangement: the fraction $p(n_t)$ of testing windows containing both the small and large numbers n_t of inclusions are diminished. Obviously, the descriptor $p(n_t)$ is a more sensitive measure of the local statistical homogeneity of the configuration analyzed than the RDF $g(r)$ is.

In Fig. 4 the statistical descriptors $g(r)$ estimated from experimental data are presented. One analyzed the single sample s_{11} from the specimen S_1 ($s_{1i} \subset S_1, i = 1, \ldots, 10$) containing 1800 fibers, the results obtained by the averaging over 10 samples $s_{1i} \subset S_1$ and $s_{2i} \subset S_2$ ($i = 1, \ldots, 10$) as well as the result of averaging over 10 specimens S_j, ($j = 1, \ldots, 10$) of materials produced by the different technological regimes each of them contains 10 samples. As can expected, the increasing of samples treated leads to the smoothness of the curves $g(r)$. In Fig. 5 the histograms of distributions of fibers in a tested window with the size $R_t = 3.1a$ are presented for the averaging over the configurations simulated by the HCSM as well as the averaging over the 100 experimental samples containing 1800 fibers each. As can be seen, the HCSM generates significantly more homogeneous and mixed arrangement then the real slightly clustered structures (compare with Fig. 3): the fractions $p(n_t)$ of testing windows containing both the small and large numbers n_t of inclusions decrease.

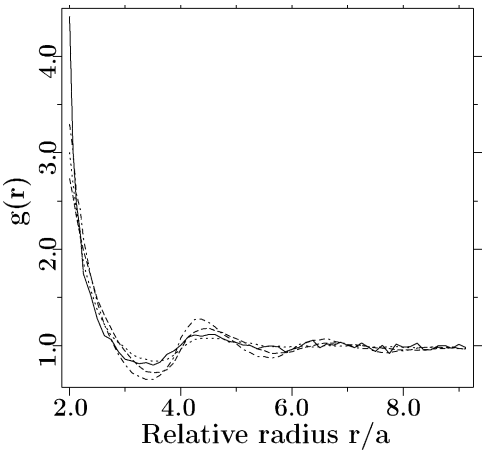

Fig. 2. The RDF $g(r)$ vs relative radius r/a estimated by the HCM at $c = 0.55$ (—) and $c = 0.5$ (···), and by HCSM at $c = 0.55$ (-·-·-) and $c = 0.5$ (- - -).

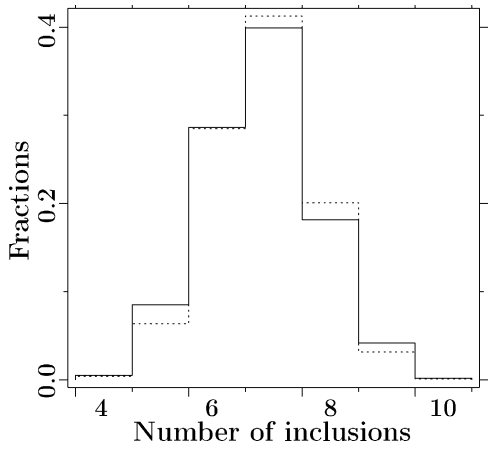

Fig. 3. Histogram of fractions $p(n_t)$ of testing window containing n_t inclusions generated by the HCM (solid curve) and by the HCSM (dotted curve).

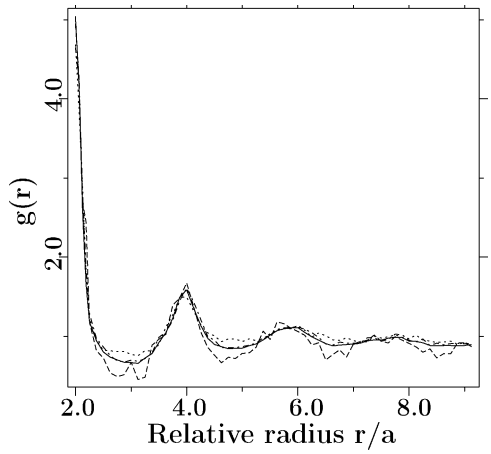

Fig. 4. The RDF $g(r)$ vs relative radius r/a estimated from experimental data for: a single sample s_{11} (dashed curve), averaged over 10 samples s_{1i}, $(i = 1, \ldots, 10)$ (dotted curve), at $c = 0.65$, averaged over 10 samples s_{2i}, $(i = 1, \ldots, 10)$ (dot-dashed curve), averaged over ten specimens produced by the different technological regime and containing ten samples each (solid curve).

The Monte Carlo shaking process is both the most structurally influential and, computationally, the most intensive part of the whole packing process. The duration of this phase, which can be measured in terms of the number of Monte Carlo steps per particle, N^{MC}/N, can be changed by varying of the size of the shake up window and the frequency ratio of the alternation of the processes between generation of a new particle and the shaking. However, the results of total simulation are not related trivially to the details of the separate stages. In Fig. 6 we have plotted for one of plausible set of input parameters, the area fraction vs the duration of the Monte Carlo simulation N^{MC}/N. Only at low particle concentrations $c < 0.52$ does the HCM allow us to generate the random packing faster than the HCSM. As the packing density increases from 0.52, the proportion of non-accepted trial generations dramatically increases in the vicinity of the jamming limit and equals, for example, 99.998% at $c = 0.5445$ and $N = 3130$ with a CPU time of 5 h for a

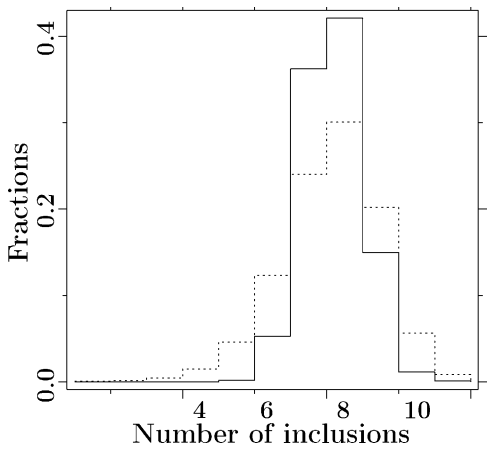

Fig. 5. Histogram of fractions $p(n_t)$ of testing window containing n_t fibers: generated by the HCSM at $N = 3700$, $N_t = 3.1a$ (solid curve), averaged over 100 samples (dotted curve).

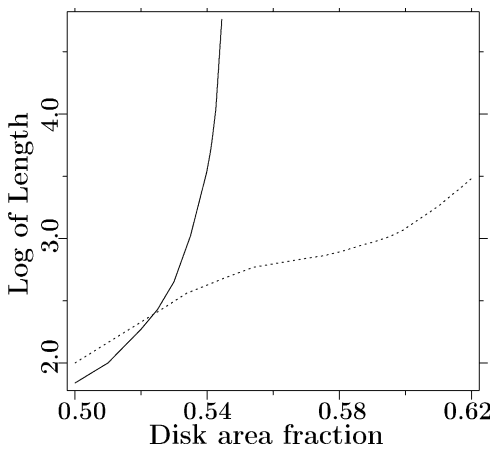

Fig. 6. Length of Monte Carlo simulation N^{MC}/N vs an area fractions c appropriate to the HCM (solid curve) and to the HCSM (dotted curve).

PC with a 644 MHz processor. At $c \approx 0.65$, the advantage of the HCSM over the HCM in creating more homogeneous configurations degenerates (see Fig. 3). Additional shortcomings are the absence of the testing windows with a small numbers of particles and a finite empty volume with a diameter of more than $2a$. Thus, the HCSM stumbles over an intrinsic obstacle in the form of a jamming limit $c^{HCHM} \approx 0.67$. This limit is more "fuzzy" than the jamming limit for the HCM $c^{HCM} = 0.55$. Forthcoming expansion of the particle concentration is possible through the utilization of the growth of the particle radius considered in Section 3.5.

3.4. Initially periodic shaking model

The periodic lattice packing Λ

$$\mathbf{x_m} = m_1\mathbf{e}_1 + m_2\mathbf{e}_2 \tag{3.6}$$

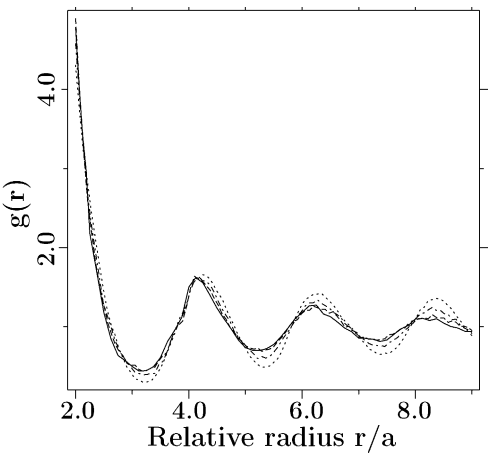

Fig. 7. The RDF $g(r)$ vs relative radius r/a estimated by the IPSM at $c = 0.65$, $N = 3700$: 150 shaking (solid curve), 100 shaking (dashed curve), 30 shaking (dot-dashed curve), 10 shaking (dotted curve).

of centers of the disks with the radius a were chosen as an initial system. Here $\mathbf{e}_l$ $(l = 1, 2)$ are linearly-independent vectors, $\mathbf{m} = (m_1, m_2)$ are integer-valued coordinates of mode $\mathbf{m}$ in the basis $\mathbf{e}_l$ which are equal in modulus to $|\mathbf{e}_l|$. In particular, for orthogonal basis $\mathbf{e}_1 = (1, 0)^\top$, $\mathbf{e}_2 = (0, 1)^\top$ and for integer set $(m_1, m_2) \in Z^2$ independent of one another, the lattice Λ defines a square packing. The basis $\mathbf{e}_1 = (0.5, 0)^\top$, $\mathbf{e}_2 = (0, \sqrt{3}/2)^\top$ with the coefficients m_l $(l = 1, 2)$ which are either all even or odd, leads to a triangular packing.

The rearrangement of initially periodic structures is conducted by the shaking procedure described in Section 3.3. The statistical parameters $g(r)$, $N^{\mathrm{nd}}(r)$ are estimated by the averaging analysis of a few global shakings allowing inclusion configurations to be generated that are more homogeneous and well-mixed. Stabilization of estimations of $g(r)$, $N^{\mathrm{nd}}(r)$ with increased numbers of global shakings leads to convergence of the shaking process. One disadvantage of this is that there is no guarantee that the initially periodic structure will be completely "destroyed" by the shaking. This deficiency is overcome by using the HCSM. The advantage of the present model is that a fixed concentration of inclusions negates the use of other procedures, such as an incrementing of the number of inclusions or increasing the inclusion radii.

Fig. 7 shows $g(r)$ as estimated by the Initially periodic shaking model (IPSM) with an initially triangular packing of inclusions and different numbers of global shakings ($c = 0.65$). As can be seen from the figure, the estimate for the RDF becomes stable if the number of global shakings is more than 50; in these situations the CPU time for one global shaking equals 10^3 s at $N = 3700$, $R_t = 3.1a$. Comparison of $g(r)$ estimated by IPSM with initial triangular and square packing of inclusions at 100 global shakings as well as by the HCSM was performed also at $c = 0.65$. From the figure there is reason to believe that a sufficiently intensive shaking process would eliminate the sensitivity of the results obtained for the concrete algorithm of the simulation of the random inclusion ensemble as well as on the initial arrangement of inclusions. Shubin (1995) has drawn the similar conclusions, in researching the close 3D packing of different initially periodic configuration of hard spheres.

3.5. Collective rearrangement model

Just for completeness we will briefly introduce the CRM accompanied by the shaking procedure. We start with a unit square $(0, 0)$ and its periodically located neighbors labeled by the duplet of integer numbers $\alpha = (\alpha_1, \alpha_2) \in Z^+$ where $\alpha_1, \alpha_2 = 0, \pm 1$. N random points $\mathbf{x}_i$ $(i = 1, \ldots, N)$ in the central square periodically

reflected into the neighboring squares are assigned to the initial velocities $\mathbf{v}_i = (v_{i1}, v_{i2})$ whose components are independently distributed at random between -1 and $+1$ and to the uniformly growing inclusions with the radii $a(t) = a_0 t$. The centers of the inclusions move according to the equations

$$\frac{\mathrm{d}\mathbf{x}}{\mathrm{d}t} = \mathbf{v}_i \tag{3.7}$$

with a discontinuous change of the vectors $\mathbf{v}_i$ at the moment the the particle exits through a face of a central square as well as during collisions with other inclusions.

The collision time is obtained from the condition that the separation distance is the current diameter, that for the inclusions v_i and v_j is

$$|\mathbf{x}_i + \mathbf{v}_i\Delta t - \mathbf{x}_j - \mathbf{v}_j\Delta t| = (a_0 t + a_0\Delta t). \tag{3.8}$$

In the case of the collision, the smaller positive root Δt of Eq. (3.8) defines the collision time τ_{ij}. If the collision takes place between the inclusions v_i and v_j from central and neighboring squares (e.g. identified by (−1,0)), respectively, then $\mathbf{x}_j$ in Eq. (3.8) should be replaced by $\mathbf{x}_j + (-1, 0)$ with a subsequent estimation of a collision time τ_{ij}. The exit time τ_i^Γ is estimated as the smallest positive time for exiting of the inclusion v_i being considered through the one of sides of the central square. The determination of $\Delta t_* = \min(\tau_{ij}, \tau_i^\Gamma)$ allows possible the estimation of the new inclusion radii $a_0(t + \Delta t_*)$ and the identification of either colliding (v_{i^*} and v_{j^*}) or exiting (v_{i^*}) inclusions for which the new velocities and locations are re-estimated. For all other inclusions the position vectors are updated according to Eq. (3.7): $\mathbf{x}_i \to \mathbf{x}_i + \mathbf{v}_i\Delta t$. For these inclusions $\Delta t = \Delta t_*$ and velocities $\mathbf{v}_i$ remain unchanged. In addition, the collision and exit times are corrected $\tau_{ij} \to \tau_{ij} - \Delta t_*$ and $\tau_i^\Gamma \to \tau_i^\Gamma - \Delta t_*$, respectively. The details of the re-estimation of velocities for the inclusions v_{i^*} and v_{j^*} based on the conservation laws of the momentum and energy can be found in Lubachevsky et al. (1991), and Knott et al. (2001).

Up to this point, a single step of the CRM has been defined. Repeating this step leads to the close packing demonstrated by Lubachevsky et al. (1990). However, because our goal is different (i.e. the simulation of well-mixed, random structures over a complete range of inclusion concentrations), further corrections to the algorithm were necessary. The algorithm is modified so that after a few repetitions estimating new velocities for the colliding inclusions, the procedures of (A) generating new inclusions in low-density testing windows and, (B) inclusion shaking (described in Section 3.3) are carried out.

Both experiments and simulations suggest a transition between random and ordered configurations in the vicinity of a density $c \approx 0.8$ (see e.g. Rankenburg and Zieve, 2001). The packing density increases much more slowly beyond this point. The understanding of this transition is more obvious after quantitative analysis given in Figs. 8 and 9 showing the RDFs $g(r)$ estimated by the modified CRM for different disk concentrations $c = 0.60$–0.75 and $c = 0.75$–0.90, respectively. As can an be seen, for high disk concentrations the plot of the RDF has a second peak which is characteristically split as was observed in the experimental packing (see e.g. Murata et al., 1996; Cargill, 1994). The split peak demonstrates the presence of large clusters with close triangular disk packing (see e.g. Turnbull and Cormia, 1960). In order to analyze the plots $g(r) \sim r$ in Fig. 9 we will compare the coordinates of their peaks with the analogous peaks for close triangular and square packing. A distinguishing characteristic of the last regular packing is the presence of "fixed" peaks corresponding to $r = 2a$, $4a$, $6a$, ..., and "floating" subpeaks, the location of which depend on the specific structure of the unit cell. For the triangular and square packing the coordinates of the subpeaks are $r = 3.46a$, $5.32a$, ..., and $r = 2.83a$, $4.44a$, $6.3a$, ..., respectively. Imperfection, both in the identification of the disk centers and in the lattice itself, broaden the peaks and raise the heights of the intervening values. Thus, one can presuppose that the second subpeak in Fig. 9 at $r = 3.47a$ is caused by the influence of local ordering in the form of clusters with the triangular structure.

It should be mentioned that the modified CRM is not as optimal as the original CRM for modeling close-packing configurations simply because the added procedure of random shaking is just focused on the

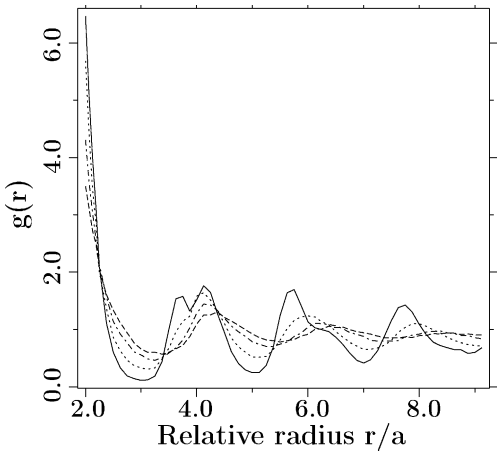

Fig. 8. The RDF $g(r)$ vs relative radius r/a estimated by the modified CRM at $c = 0.60$ (dashed curve), $c = 0.65$ (dot-dashed curve), $c = 0.70$ (dotted curve), $c = 0.75$ (solid curve); N grows from 799 to 811.

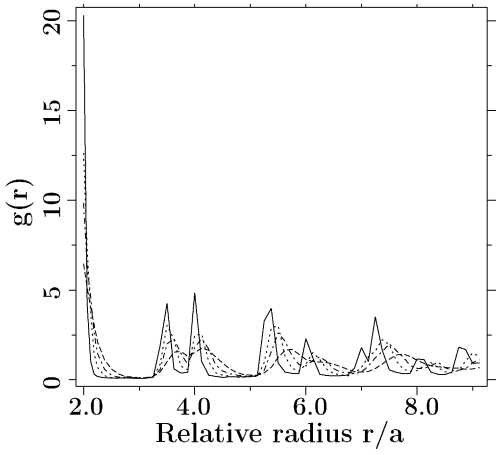

Fig. 9. The RDF $g(r)$ vs relative radius r/a estimated by the modified CRM at $N = 811$ and $c = 0.90$ (solid curve), $c = 0.85$ (dotted curve), $c = 0.8$ (dot-dashed curve), $c = 0.75$ (dashed curve).

"destruction" of dense "locked" local configurations in some testing windows, leading to the generation of highly homogeneous and mixed structures. In relation to the last statement, it should be mentioned that the work by Döge (2000) combines various Metropolis–Hastings algorithms to obtain a simulation algorithm with good mixing properties. However, the comparison of Fig. 2 by Döge (2000) for the RDF $g(r)$ with $c = 0.65$ and $c = 0.735$ indicates that his $g(r)$ function reflects more order. On the other hand, the modification of the known simulation protocol by adding a shaking procedure has some additional benefits. So, in the HCM, CRM, and sequential generation models, the parameters and functions are calculated only from one simulation of the generated configuration. These data should be considered as merely a single realization of such a random generation process. In order to provide statistically more reliable results it would be necessary to average several realizations. However, this repeating procedure is not necessary in the protocols accompanied by a shaking procedure because a configuration generated by a few global

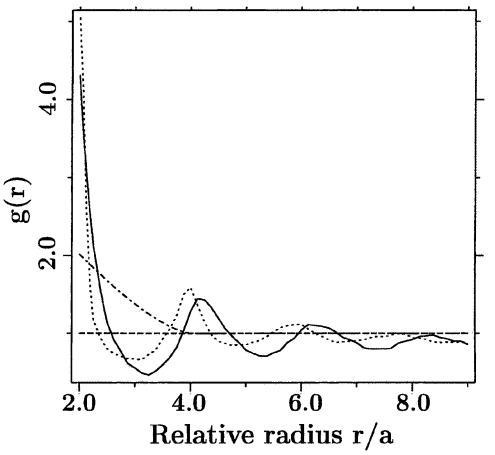

Fig. 10. The RDF $g(r)$ vs relative radius r/a estimated by the numerical simulation (solid curve), from experimental data (dotted curve), by the analytical approximation (3.10) (dot-dashed curve), by the well steered approximation (3.9) (dashed curve).

shakings can be regarded as a separate realization. The total computer time required for statistical analysis varies considerably with the inclusion number N as well as with the number of global shakings homogenizing the generated configuration.

In Fig. 10 we compare the RDF estimated from the experimental fiber centroid data with that from numerical simulation by the CRM, as well as the RDF represented analytically by

$$g(\mathbf{x}_i - \mathbf{x}_q) \equiv H(r - 2a), \tag{3.9}$$

$$g(\mathbf{x}_i - \mathbf{x}_q) = H(r - 2a)\left\{1 + \frac{4}{\pi}\left[\pi - 2\sin^{-1}\left(\frac{r}{4a}\right) - \frac{r}{2a}\sqrt{1 - \frac{r^2}{16a^2}}\right]H(4a - r)\right\}, \tag{3.10}$$

where H denotes the Heaviside step function, $r \equiv |\mathbf{x}_i - \mathbf{x}_q|$ is the distance between the non-intersecting inclusions v_i and v_q, and c is the area fraction of inclusions. The so-called well-stirred approximation for the RDF differs from the RDF for a Poisson distribution (3.4) by the availability of included volume with the center $\mathbf{x}_i$ where $g(\mathbf{x}_i - \mathbf{x}_q) \equiv 0$. Eq. (3.10) (see Torquato and Lado, 1992; Hansen and McDonald, 1986) takes into account a neighboring order in the distribution of the inclusions. Fig. 10 shows a good fit between RDFs estimated from experimental data and a from numerical simulation by the modified CRM and a substantial dissimilarity from the curves (3.9) and (3.10).

4. Effective elastic properties

4.1. Multiparticle effective field method

First, we will summarize the basic assumptions and the final formulae of the multiparticle effective field method (MEFM) for estimation of effective elastic moduli. For a detailed discussion and numerous references for this and related methods, the reader is referred to Buryachenko (2001a).

Assume stresses and strains are related to each other via the constitutive equation

$$\boldsymbol{\sigma}(\mathbf{x}) = \mathbf{L}(\mathbf{x})\boldsymbol{\varepsilon}(\mathbf{x}), \tag{4.1}$$

where $\mathbf{L}$ is the fourth-order elasticity tensor, which for isotropic materials is given by $\mathbf{L} = (3k, 2\mu) \equiv 3k\mathbf{N}_1 + 2\mu\mathbf{N}_2$, $\mathbf{N}_1 = \boldsymbol{\delta} \otimes \boldsymbol{\delta}/3$, $\mathbf{N}_2 = \mathbf{I} - \mathbf{N}_1$, k and μ are the bulk and shear modulus, respectively; $\boldsymbol{\delta}$ and $\mathbf{I}$ are the unit second-order and fourth-order tensors. The local strain and stress tensors satisfy the linearized strain–displacement relations and the equilibrium equation, respectively. The homogeneous boundary conditions take place $\mathbf{u}(\mathbf{x}) = \boldsymbol{\varepsilon}^{\partial w}(\mathbf{x})\mathbf{x}$, where $\boldsymbol{\varepsilon}^{\partial w}(\mathbf{x}) = \text{const.}$, $(\mathbf{x} \in \Gamma)$ is a given symmetric tensor.

The general integral equation is known (see for references Buryachenko, 2001a)

$$\boldsymbol{\varepsilon}(\mathbf{x}) = \langle \boldsymbol{\varepsilon} \rangle(\mathbf{x}) + \int \mathbf{U}(\mathbf{x} - \mathbf{y})[\boldsymbol{\eta}(\mathbf{y}) - \langle \boldsymbol{\eta}(\mathbf{y}) \rangle] \, \mathrm{d}\mathbf{y}, \tag{4.2}$$

where the tensor $\boldsymbol{\eta}(\mathbf{x}) = \mathbf{L}_1(\mathbf{y})\boldsymbol{\varepsilon}(\mathbf{y})$ is called the stress polarization tensor, and the notation $\langle (\cdot) \rangle$ will be used for the statistical average. The tensor of elastic properties is decomposed as $\mathbf{L}(\mathbf{x}) \equiv \mathbf{L}^{(0)} + \mathbf{L}_1(\mathbf{x}) = \mathbf{L}^{(0)} + \mathbf{L}_1^{(m)}(\mathbf{x})$. Here and in the following, the upper index $^{(m)}$ $(m = 0, 1)$ indicates the components and the lower index i indicates the individual inclusions; $v^{(0)} = w \setminus v^{(1)}$, $v^{(1)} \equiv \cup v_i$, $V(\mathbf{x}) = \sum V_i(\mathbf{x})$, and $V^{(1)}(\mathbf{x})$ is a characteristic function of $v^{(1)}$ $(i = 1, 2, \ldots)$. The integral operator kernel $\mathbf{U}(\mathbf{x} - \mathbf{y}) \equiv \nabla\nabla\mathbf{G}(\mathbf{x} - \mathbf{y})\mathbf{L}^{(0)}$ is defined by the Green tensor $\mathbf{G}$ of the Lame' equation of a homogeneous medium with an elasticity tensor $\mathbf{L}^{(0)}$: $\nabla\{\mathbf{L}^{(0)}[\nabla \otimes \mathbf{G}(\mathbf{x}) + (\nabla \otimes \mathbf{G})^{\top}]/2\} = -\boldsymbol{\delta}\delta(\mathbf{x})$; $\delta(\mathbf{x})$ is the Dirac delta function.

After conditional statistical averaging Eq. (4.2) turns into an infinite system of integral equations. In order to close and approximately solve this system we now apply the MEFM hypotheses

H 1. Each inclusion v_i has an ellipsoidal form and is located in the field

$$\bar{\boldsymbol{\varepsilon}}(\mathbf{y}_i) \equiv \bar{\boldsymbol{\varepsilon}}(\mathbf{x}_i)(\mathbf{y} \in v_i) \tag{4.3}$$

which is homogeneous over the inclusion v_i.

H 2. Each pair of the inclusions v_i and v_j is located in an effective field $\hat{\boldsymbol{\varepsilon}}(\mathbf{x})_{i,j}$ and

$$\langle \hat{\boldsymbol{\varepsilon}}(\mathbf{x})_{i,j} \rangle_k = \langle \bar{\boldsymbol{\varepsilon}}_k \rangle(\mathbf{x}) = \text{const.} \quad (\mathbf{x} \in v_k, k = i, j). \tag{4.4}$$

According to hypothesis **H1** and to Eshelby's theorem we get $(\mathbf{x} \in v_i)$

$$\boldsymbol{\varepsilon}(\mathbf{x}) = \mathbf{A}\bar{\boldsymbol{\varepsilon}}(\mathbf{x}), \quad \bar{v}_i\boldsymbol{\eta}_i(\mathbf{x}) = \mathbf{R}\bar{\boldsymbol{\varepsilon}}(\mathbf{x}), \tag{4.5}$$

where $\mathbf{R} = \bar{v}_i\mathbf{L}_1^{(1)}\mathbf{A}$, $\mathbf{A} = [\mathbf{I} + \mathbf{P}\mathbf{L}_1^{(1)}]^{-1}$ and the tensor $\mathbf{P} \equiv -\langle \mathbf{U} \rangle_{(i)}$ is associated with the well-known Eshelby tensor $\mathbf{S}$ by $\mathbf{S} = \mathbf{P}\mathbf{L}^{(0)}$. Hereafter $\boldsymbol{\eta}_i \equiv \langle \boldsymbol{\eta}(\mathbf{x})V_i(\mathbf{x}) \rangle_{(i)}$ is an average over the volume of the inclusion v_i (but not over the ensemble), $\langle (\cdot) \rangle_i \equiv \langle \langle (\cdot) \rangle_{(i)} \rangle$, and the tensors

$$\mathbf{T}_i(\mathbf{y} - \mathbf{x}_i) = \begin{cases} -(\bar{v}_i)^{-1}\mathbf{P}_i, & \mathbf{y} \in v_i, \\ \langle \mathbf{U}(\mathbf{y} - \mathbf{x})V_i(\mathbf{x}) \rangle_{(i)}, & \mathbf{y} \notin v_i, \end{cases} \quad \mathbf{T}_{ij}(\mathbf{x}_i - \mathbf{x}_j) = \langle \mathbf{T}_i(\mathbf{z} - \mathbf{x}_i) \rangle_{(j)} \tag{4.6}$$

$(\mathbf{z} \in v_j \neq v_i)$ have analytical representations for the spherical inclusions in an isotropic matrix. In the framework of the hypothesis **H1**, the Eq. (4.2) is reduced to the equation with respect to the stress polarisation tensor

$$\boldsymbol{\eta}(\mathbf{x}) = \mathbf{R}\langle \boldsymbol{\varepsilon} \rangle + \int \mathbf{R}\mathbf{U}(\mathbf{x} - \mathbf{y})[\boldsymbol{\eta}(\mathbf{y})V(\mathbf{y}|; v_i, \mathbf{x}_i) - \langle \boldsymbol{\eta}(\mathbf{y}) \rangle] \mathrm{d}\mathbf{y}, \tag{4.7}$$

where $V(\mathbf{y}|; v_i, \mathbf{x}_i) = \sum_j V_j(\mathbf{y}) - V_i(\mathbf{y})$, $j = 1, 2, \ldots$

The hypotheses **H1**, **H2** can be used for an approximate solution of Eq. (4.2) and subsequent estimation of effective elastic moduli in the overall constitutive equation $\langle \boldsymbol{\sigma} \rangle = \mathbf{L}^* \langle \boldsymbol{\varepsilon} \rangle$:

$$\mathbf{L}^* = \mathbf{L}^{(0)} + \mathbf{YR}n, \quad \mathbf{Y}^{-1} = \mathbf{I} - \int \mathscr{T}_{iq}(\mathbf{x}_i - \mathbf{x}_q)\,\mathrm{d}\mathbf{x}_q, \tag{4.8}$$

$$\mathscr{T}_{iq}(\mathbf{x}_i - \mathbf{x}_q) \equiv \mathbf{R}_i n\big\{\mathbf{T}_{iq}(\mathbf{x}_i - \mathbf{x}_q)[\mathbf{Z}_{qi} + \mathbf{Z}_{qq}]g(r) - \mathbf{T}_i(\mathbf{x}_i - \mathbf{x}_q)\big\}, \tag{4.9}$$

where $r = |\mathbf{x}_q - \mathbf{x}_i|$, and the matrix elements $\mathbf{Z}_{qi}$, $\mathbf{Z}_{qq}$ are non-diagonal and diagonal elements, respectively, of the binary interaction matrix $\mathbf{Z}$ for the two inclusions v_q and v_i with the elements of the inverse matrix

$$(\mathbf{Z}^{-1})_{iq} = \mathbf{I}\delta_{iq} - (1 - \delta_{iq})\mathbf{R}_q\mathbf{T}_{iq}(\mathbf{x}_i - \mathbf{x}_q). \tag{4.10}$$

Thus, the effective elastic moduli $\mathbf{L}^*$ explicitly depend on the RDF $g(r)$ and the volume concentration $c = n\bar{v}_i$ of inclusions. The neglect of the binary interaction of inclusions

$$\mathbf{Z}_{iq} = \mathbf{I}\delta_{iq} \tag{4.11}$$

reduces the formula (4.7) for the effective elastic moduli to the analogous relation obtained by Mori–Tanaka (MT) method which is invariant to the RDF $g(r)$.

In order to demonstrate the comparison of the available experimental data with the predicting capability of the proposed method, we will consider the estimation of the effective elastic moduli $\mathbf{L}^*$ (4.8). Assume the matrix is epoxy resin ($k^{(0)} = 4.27$ GPa and $\mu^{(0)} = 1.53$ GPa) which contains identical circular glass fibers ($k^{(1)} = 50.89$ GPa and $\mu^{(1)} = 35.04$ GPa). Four different RDF for the inclusions will be examined (see Torquato and Lado, 1992; Hansen and McDonald, 1986). As can be seen from Fig. 11 the use of the approach (4.7) and (4.10) based on the quasi-crystalline approximation (4.10) (also called MT approach) leads to an underestimate of the effective shear modulus by 1.85 times for $c = 0.7$ compared with the experimental data. Much better approximations are given by the MEFM (4.7)–(4.9) which shows good agreement with the experimental data provided by Lee and Mykkanen (1987). In the MEFM model, the best fit is obtained using the RDF simulated by the modified CRM.

Let us now demonstrate an application of the theoretical results by considering an isotropic composite made of an incompressible isotropic matrix, filled with rigid disc inclusions of one size ($n = 1$). This example was chosen deliberately because it provides the maximum difference between predictions of effective elastic response, as estimated by the various methods. In Fig. 12 the most advanced micromechanical model

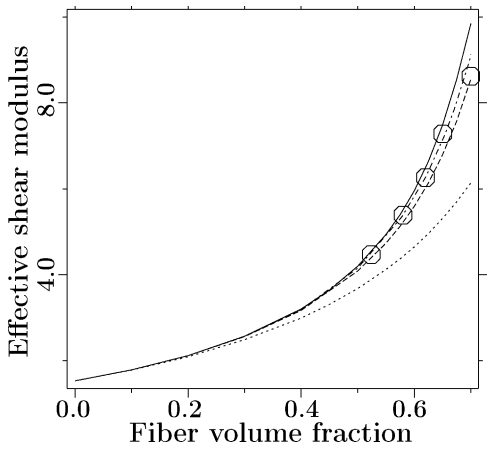

Fig. 11. Variation of the effective shear modulus μ^* as a function of a concentration of the inclusions c. Experimental data (○) and curves calculated by Eqs. (4.7)–(4.9) and (3.10) (solid line), by (4.7)–(4.9) and (3.10) with the RDF simulated by the modified CRM (-·-·-), by Eqs. (4.7)–(4.9) and (3.9) (dashed curve), by the MT method (···), and by the boundary element method of the hexagonal fiber packing by Eischen and Torquato (1993).

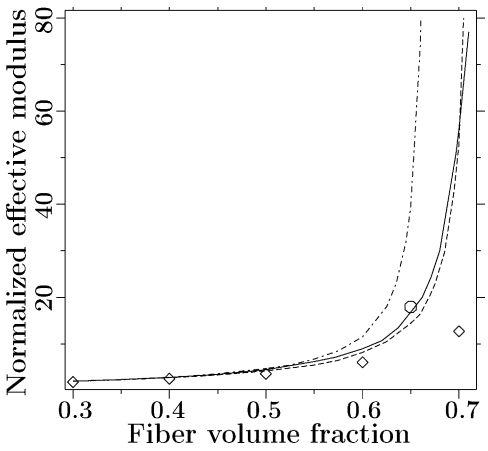

Fig. 12. Variation of the relative effective shear modulus $\mu^*/\mu^{(0)}$ as a function of a concentration of the inclusions c estimated by Eqs. (4.7)–(4.9) and (3.10) (-·-·-), by (4.7)–(4.9) with the RDF simulated by the modified CRM (solid curve), by (4.7)–(4.9) and (3.9) (dashed curve), and by (4.7)–(4.9) with experimentally estimated RDF (○).

(4.7)–(4.9) is analyzed for the effect of choosing different RDFs. As can be seen, the effective shear moduli can be differ by a factor of two or more depending on the chosen RDF. In so doing, the RDF simulated by the modified CRM provides the estimations of $\mu^*/\mu^{(0)}$ that are very close to those obtained by the real RDF at $c = 0.65$. It is interesting that all RDF lead to infinite values of $\mu^*(c)$ for large values of c, but the simulated RDF provides a limiting upper value of $c = 0.72$.

4.2. Some related methods used second order microstructure statistical information

It would be interesting to compare (at least a qualitative sense) the MEFM with some related methods of prediction of effective moduli that account for higher-order microstructural information. So, in the elegant method by Torquato (1997, 1998) the exact series expansions for the effective stiffness tensor were obtained for macroscopically anisotropic, d-dimensional, two-phase composite media in powers of the "elastic polarization". The method departs from previous treatments by introducing an integral equation for the "cavity" strain field which coincides with our notations for the spherical inclusions with the effective field $\bar{\boldsymbol{\varepsilon}}(\mathbf{x}) = \mathbf{A}^{-1}\boldsymbol{\varepsilon}(\mathbf{x})$ introduced by Eq. (4.5). At the next step the equation for the cavity strain field (or the effective field) was recast in terms of the elastic polarization tensor $\boldsymbol{\eta}$ (4.3), where the driving term $\mathbf{R}\langle\boldsymbol{\varepsilon}\rangle$ (called the external stress polarization by Buryachenko, 2001a) was obtained as an extraction of the Eshelby solution for a single inclusion in the infinite matrix subjected to the field $\langle\boldsymbol{\varepsilon}\rangle$. After that the analog of Eq. (4.3) used by Torquato (1997) can be solved by the iteration method similarly to the perturbation method or the method of correlation appropximation (see Beran and McCoy, 1970). In so doing the driving term of Eq. (4.3), which is the external strain polarization factor $\mathbf{R}\langle\boldsymbol{\varepsilon}\rangle$, is chosen as an initial approximation. The last choice is better than that in the classical method of correlation approximation with the initial approximation $\langle\boldsymbol{\varepsilon}\rangle$. However, Torquato (1997) has proposed a much better choice, and extracted in Eq. (4.2) as a driving term not only the Eshelby solution $\mathbf{R}\langle\boldsymbol{\varepsilon}\rangle$ for a single inclusion but also the solution corresponding to one of the Hashin and Shtrikman (1963) bounds for the composite material that makes it possible to analyze any contrasting of the components. The final explicit representations for the effective moduli $\mathbf{L}^*$ depend on the N-point correlation functions $S_N^{(i)}(\mathbf{y}^N)$, and the interactions of different inclusions is not directly taken into account. In essence, this prospective idea by Torquato (1997) of the extraction of Hashin–Shtrikman's solution as a driving term was developed by Buryachenko (2001b) in his combined

MEFM-perturbation method in which the scheme by Torquato (1997) of the iteration approximation of the integral operator involved was directly accompanied by the solution for the binary interacting inclusions explicitly depending on the RDF $g(r)$. Buryachenko (2001b) demonstrated the advantage of the standard MEFM over the combined MEFM-perturbation method through the comparison with experimental data for the Newtonian suspensions of identical spherical rigid inclusions. It should be mentioned that to obtain concrete numerical estimations of $\mathbf{L}^*$ by the use of exact formulae by Torquato (1997), it is necessary to know a complete set of the functions $S_N^{(i)}(\mathbf{y}^N)$ $(N \to \infty)$. The last is practically improbable because, to the authors knowledge, the systematic estimations even of three-pont functions $S_3^{(i)}(\mathbf{y}^3)$ for the real microstructures were not conducted, although the necessary microstructural parameters were estimated for the hexagonal array of cylinders by Eischen and Torquato (1993). Underestimating of effective elastic properties of the hexagonal fiber packing with respect to the random one (see Fig. 12) is consistent with the similar comparison of 3D random and regular sphere packing. But in the case of the limitation of the microstructural knowledge just by two-point function $S_2^{(i)}(\mathbf{y}^2)$ (or $g(r)$), the estimations by Torquato (1997) degenerate to one of the Hashin–Shtrikman boundaries or MT estimations that is worse than the MEFM's evaluations (see Fig. 11 and Buryachenko, 2001a,b) using the same information for the function $g(r)$.

Another alternative version of the multiparticle method deserves more attention. It is the method proposed by Ju and Chen (1994a,b) for a linear problem of estimation of the effective elastic moduli which was extensively developed by themselves and their coauthors as applied to a wide class of non-linear problems such as estimation of second moments of stresses as well as plasticity and damage phenomena (see the last papers Lee and Simunovic, 2000; Ju and Lee, 2001; Ju and Sun, 2001; Ju and Zhang, 2001 where the previous references can be found). However, the internal inconsistency of the mentioned source approach of the estimation of both the effective elastic properties and the second moment of stresses was discussed in detail by Buryachenko (2001a,b) (where the references on additional analyses can be found) and, because of this, the correctness of including these approaches into the non-linear approaches of both plasticity and damage phenomena is questionable.

It should be mentioned that insensitivity of the estimations of $\mathbf{L}^*$ on the second-order functions ($S_2^{(i)}(\mathbf{y}^2)$ or $g(r)$) in the case of the quasi-crystalline approximation (4.10) takes place just for the local problem of the estimation of $\mathbf{L}^*$ with homogeneous external loading. In the case of the inhomogeneous loading ($\langle \boldsymbol{\varepsilon} \rangle(\mathbf{x}) \neq$ const.), the overall constitutive equations are described by either the differential or integral effective operator explicitly depending on the functions either $S_2^{(i)}(\mathbf{y}^2)$ or $g(r)$ even in the case of the assumption (4.10) (see for references and details Buryachenko and Pagano, in press). However, the estimations obtained by the MEFM through directly taking the effect of binary interacting inclusion into account are more sensitive to the function $g(r)$ than ones obtained in the framework of the quasi-crystalline approximation (4.10).

5. Concluding remarks

It should be mentioned that for computer-simulated configurations, the particle reorganization induced by shaking is subjected only to geometrical constraints, whereas for real structures the packing is far more complicated and controlled by elastic, hydrodynamic, and cohesive forces etc. Our simulation technique is able to isolate the fundamental geometrical constraints from other physico-mechanical and chemical effects and therefore the results provide a valuable benchmark for evaluating sophisticated packing schemes used in the modeling of real composite materials. It was shown that a sufficiently intensive shaking process leads to the stabilization of a statistical distribution of the simulated structure that is most homogeneous, highly-mixed and protocol independent (in sense that the statistical parameters estimated do not depend on the basic simulated algorithm such as HCM, CRM or other). The arguments justified the last statement are plausible rather than rigorous and require additional investigations.

It is known that taking only one point probability density (volume fraction) into account can provide only a rough estimation of bounds of effective properties and statistical averages of stresses in the constitutive equations of composite materials. More informative characteristics of the point set are obtained using statistical second-order quantities (such as two-point probability density, second-order intensity function, and NND) which examine the association of points relative to other points. A few contributions have paid attention to the application of these statistical distributions for generation of concrete realizations of the locations of a finite number of interacting inclusions with subsequent analyses (see e.g. Ghosh et al., 1997; Pyrz and Bochenek, 1998). More rigorous estimations of the statistical average of stress fields in the constituents and effective elastic moduli are based on the statistical averaging of random integral equations involved for an infinite number of inclusions whose configurations are described by statistical second-order functions (see for references Buryachenko, 2001a; Torquato, 2002). In particular, in the current paper we demonstrated the strong dependence of effective moduli on the concrete form of RDF and demonstrated strong differences between apparently similar distributions.

It should be mentioned, however, that estimation of effective elastic moduli is a linear problem with respect to the stress field analyzed which makes the analysis less sensitive to the local stress distribution than non-linear micromechanical problems such as elastoplastic deformation, fracture, and fatigue of composite materials. In this respect, Buryachenko (2001a) estimated the second moment of stresses averaged over the volume of the constituents by the RDF, for application in the analysis of a wide class of non-linear problems. These estimations of the second moment of stresses averaged over the volume of components are defined by both the random stress fluctuations in the components and the inhomogeneity of the stress fields in the constituents that can not be separated in the framework of the method proposed. It should be mentioned that the admission of the hypothesis (4.10) of necessity leads to the absence of stress fluctuations inside the homogeneous ellipsoidal inclusions as opposed to the estimations by the MEFM. Moreover, just a stress fluctuation inside the inclusions defines the stress fluctuations at the interface between the matrix and inclusions that, in turn, plays a fundamental role in the process of interface localization phenomena, such as plasticity (see for references Buryachenko et al., 2002) and failure (see e.g. Tandon et al., submitted for publication).

There are a few models (see for references He and Ekere, 2001) based on the idea that at high inclusion concentrations, the effective properties are dominated by the interaction forces between neighboring particles that are proportional to δ^{-1} where δ is the ratio of the mean gap between neighboring particles to particle diameter. Obviously, the use of the average value $\delta \equiv \langle N^{\rm nd}\rangle/(2a)$ instead of random distribution $N^{\rm nd}$ leads to the loss of statistical information concerning the microtopology of the composite and is conceptually questionable because estimating the average of the output parameter (such as effective modulus) by the use of the average of the random input parameter (such as nearest neighbor distance) is essentially a non-linear problem. The approach by Pyrz (1994) based on the elastic solution for two interacting inclusions in an infinite matrix with subsequent averaging by the NND is a distinct improvement because it is more sensitive to the local configuration of inclusions. In so doing, the crude assumption by Pyrz (1994) that two inclusions are subjected to the field $\langle\hat{\boldsymbol{\varepsilon}}(\mathbf{x})_{i,j}\rangle \equiv \langle\boldsymbol{\varepsilon}\rangle$ (4.4) can be relaxed by the use of more accurate estimations by Buryachenko (2001a,b) of the correlation function of the effective field $\langle\hat{\boldsymbol{\varepsilon}}(\mathbf{x})_{i,j}\rangle$ acting on two inclusions v_i and v_j fixed in the composite material. However, more detailed realization of this scheme is beyond the scope of the current study and will be considered in forthcoming publications by the authors.

For researchers the statistical description of statistically homogeneous structures is a fascinating subject studied in many papers and books. In contrast, the analogous analyses for statistically inhomogeneous media such as clustered and functionally graded materials are posing annoying problems. In such a case, the ergodicity fails, and ensemble and volume averages do not coincide. The degenerate case of this material is a random matrix composite bounded in some directions as well as the effective composites media for the inclusions are located in a region bounded in some directions, although unrestrictedness of the domain of inclusion locations does not preclude statistical inhomogeneity. For example, any laminated composite

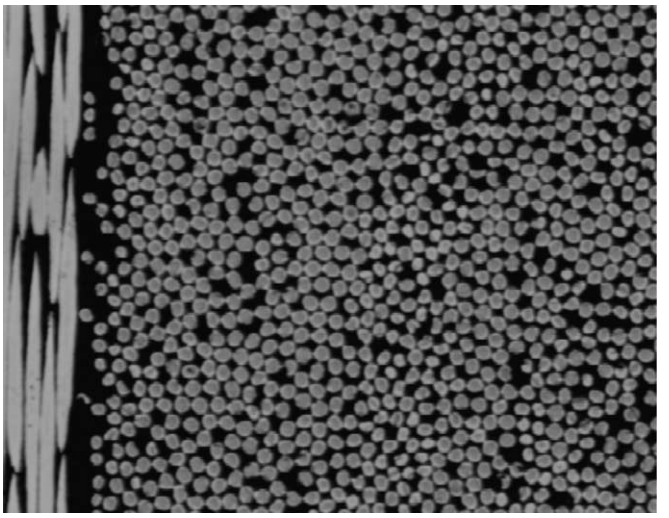

Fig. 13. Fragment of the original micrograph of fiber composite material microstructure near the boundary between two plies with the different orientation of alligned fibers.

materials randomly reinforced by aligned fibers in each ply, are a statistically inhomogeneous (or functionally graded) material (see Fig. 13). There are just a few theoretical papers which study structures with a gradient or with clustered objects (Hahn et al., 1999; Quintanilla and Torquato, 1997). So, Quintanilla and Torquato (1997) proposed statistical descriptions for particulate, statistically inhomogeneous two-phase random media by the use of the theory of a general Poisson process (see Stoyan and Stoyan, 1994) and estimated for some simulated fully penetrable (Poisson distribution) spheres the canonical n-point microstructure function, the nearest neighbor functions, and the linear-path function that, unlike the homogeneous case, will depend on their absolute positions. Usually one analyzes so-called ideal cluster materials that contain either a finite or infinite, deterministic or random ellipsoidal domain called particle clouds distributed in the composite matrix. In so doing the concentration of particles is a piecewise constant and a homogeneous one within the areas of ellipsoidal clouds and composite matrix (see Leblond and Perrin, 1999; Shan and Gokhale, 2002). The most used descriptor for the clustered and graded materials is a volume concentration of inclusions (see e.g. also Reiter et al., 1997; Suresh and Mortensen, 1998; Dao et al., 1997) which is not enough for the characterization of the micromorphology of fillers, simply because one can present other morphology with the same descriptor. However, just taking into account binary interacting inclusions effects directly dependent on the RDF allows Buryachenko (2001a) to detect some fundamentally new non-local effects for graded materials. In light of this, the further development of a statistical quantitative description for so many prospective clustered and graded materials is of profound importance in both practically and theoretically sense and will be considered in forthcoming publications by the authors.

Acknowledgements

This work was supported by AFRL/MLBC (Contract F33615-00-D-5006).

References

Barker, G.C., 1993. Computer simulation of granular materials. In: Mehta, A. (Ed.), Granular Matter—An Interdisciplinary Approach. Springer Verlag, Berlin.

Bennet, C.H., 1972. Serially deposited amorphous aggregates of hard spheres. J. Appl. Phys. 43, 2727–2734.
Beran, M.J., McCoy, J.J., 1970. Mean field variations in a statistical sample of heterogeneous linearly elastic solids. Int. J. Solid Struct. 6, 1035–1054.
Berryman, J.G., 1983. Random close packing of hard spheres and disks. Phys. Rev. A 27, 1053–1061.
Berryman, J.G., 1985. Measurement of spatial correlation functions using image processing techniques. J. Appl. Phys. 57, 2374–2384.
Bhattacharyya, A., Lagoudas, D.C., 2000. Effective elastic moduli of two-phase transversely isotropic composites with aligned clustered fibers. Acta Mechanica 145, 65–93.
Binder, K., Heerman, D.W., 1997. Monte Carlo simulation in statistical physics: an introduction. Springer, Berlin, NY.
Boudreaux, D.S., Gregor, J.M., 1977. Structure simulation of transition-metal-metalloid glasses. J. Appl. Phys. 48, 152–158.
Buryachenko, V.A., 2001a. Multiparticle effective field and related methods in micromechanics of composite materials. Appl. Mech. Rev. 54, 1–47.
Buryachenko, V.A., 2001b. Multiparticle effective field and related methods in micromechanics of random composite materials. Math. Mech. Solids 6, 577–612.
Buryachenko, V.A., Pagano, N.J., 2003. Nonlocal models of stress concentrations and effective thermoelastic properties of random structure composites. Math. Mech. Solids, in press.
Buryachenko, V.A., Rammerstorfer, F.G., Plankensteiner, A.F., 2002. A local theory of elastoplastic deformation of two-phase metal matrix random structure composites. ASME J. Appl. Mech. 69, 489–496.
Cargill III, G.S., 1994. Random packing for amorphous binary alloys. J. Phys. Chem. Solids 55, 1375–1380.
Cesarano III, J., McEuen, M.J., Swiler, T., 1995. Computer simulation of particle packing. Int. SAMPLE Technical Conf. 27, 658–665.
Cheng, Y.F., Guo, S.J., Lay, H.Y., 2000. Dynamic simulation of random packing of spherical particles. Powder Technol. 107, 123–130.
Clarke, A.S., Willey, J.D., 1987. Numerical simulation of the dense random packing of a binary mixture of hard spheres: amorphous metals. Phys. Rev. B. 35, 7350–7356.
Corson, P.B., 1974. Correlation function for predicting properties of heterogeneous materials. I. Experimental measurement of spatial correlation functions in multiphase solids. J. Appl. Phys. 45, 3159–3164.
Dao, M., Gu, P., Maewal, A., Asaro, R.J., 1997. A micromechanical study of residual stresses in functionally graded materials. Acta Mater. 45, 3265–3276.
Davis, I.L., Carter, R.G., 1989. Random particle packing by reduced dimension algorithms. J. Appl. Phys. 67, 1022–1029.
Diggle, P.J., 1983. Statistical Analysis of Spatial Point Patterns. Academic Press, NY.
Döge, G., 2000. Grand canonical simulation of hard-disc systems by simulated tempering. In: Mecke, K.R., Stoyan, D. (Eds.), Statistical Physics and Spatial Statistics: the Art of Analyzing and Modeling Spatial Structures and Patern Formation. Lecture Notes in Physics, vol. 554, Berlin.
Eischen, J.W., Torquato, S., 1993. Determining elastic behaviour of composites by the boundary element method. J. Appl. Phys. 74, 159–170.
Feder, J., 1980. Random sequential adsorption. J. Theor. Biol. 87, 237–254.
Furukawa, K., Imai, K., Kurashige, M., 2000. Simulated effect of box size and wall on porosity of random packing of spherical particles. Acta Mechanica 140, 219–231.
Ghosh, S., Mukhopadhyay, S.N., 1991. A two-dimensional automatic mesh generator for finite element analysis for random composites. Compos. Struct. 41, 245–256.
Ghosh, S., Nowak, Z., Lee, K., 1997. Quantitative characterization and modeling of composite microstructures by Voronoi cells. Acta Mater. 45, 2215–2234.
Green, P.I., Sibson, R., 1977. Computing Dirichlet tesselations in the plane. Comput. J. 21, 168–173.
Hahn, U.A., Micheletti, R., Pohlink, R., Stoyan, D., Wendrock, H., 1999. Stereological analysis and modelling of gradient sructures. J. Microsc. 195, 113–124.
Hall, P., 1988. Introduction to the Theory of Coverage Processes. John Willey & Sons, NY.
Hansen, J.P., McDonald, I.R., 1986. Theory of Simple Liquids. Academic Press, NY.
Hashin, Z., Shtrikman, S., 1963. A variational approach to the theory of the behavior of multiphase materials. J. Mech. Phys. Solids 11, 127–140.
He, D., Ekere, N.N., 2001. Structure simulation of concentrated suspensions of hard spherical particles. AIChE J. 47, 53–59.
He, D., Ekere, N.N., Cai, L., 1999. Computer simulation of random packing of unequal particles. Phys. Rev. E 60, 7098.
Hinrichsen, E.L., Feder, J., Jossang, T., 1986. Geometry of random sequential adsorption. J. Statist. Phys. 44, 793–827.
Jensen, E.B.V., 1998. Local Stereology. Word Science, Singapore.
Jodrey, W.S., Tory, M., 1985. Computer simulation of close random packing of equal spheres. Phys. Rev. A 32, 2347.
Ju, J.W., Chen, T.M., 1994a. Micromechanics and effective moduli of elastic composites containing randomly dispersed ellipsoidal inhomogeneities. Acta Mech. 103, 103–121.
Ju, J.W., Chen, T.M., 1994b. Effective elastic moduli of two-phase composites containing randomly dispersed spherical inhomogeneities. Acta Mech. 103, 123–144.

Ju, J.W., Lee, H.K., 2001. A micromechanical damage model for effective elastoplastic behavior of partially debonded ductile matrix composites. Int. J. Solids Struct. 38, 6307–6332.
Ju, J.W., Sun, L.Z., 2001. Effective elastoplastic behavior of metal matrix composites containing randomly located aligned spheroidal inhomogeneities. Part I: Micromechanics.. Int. J. Solids Struct. 38, 183–201.
Ju, J.W., Zhang, X.D., 2001. Effective elastoplastic behavior of ductile matrix composites containing randomly located aligned circular fibers. Int. J. Solids Struct. 38, 4045–4069.
Kansal, A.R., Truskett, T.M., Torquato, S., 2000. Nonequilibrium hard-disk packing with controlled orientational order. J. Chem. Phys. 113, 4844–4851.
Karlsson, L.M., Liljeborg, A., 1994. Second-order stereology for pores in translucent alumina studied by confocal scanning laser microscopy. J. Microsc. 175, 186–194.
Knott, G.M., Jackson, T.L., Buckmaster, J., 2001. Random packing of heterogeneous propellants. AIAA J. 39, 678–686.
Kondrachuk, A.V., Shapovalov, G.G., Kartuzov, V.V., 1997. Simulation modeling of the randomly nonuniform structure of powders. Two-dimensional formulation of the problem. Poroshkovaya Metallurgiya (1–2), 111–118 (in Russian. Engl. Translation. Powder Metallurgy and Metal Ceramics 36, 101–106).
König, D., Carvajal-Gonzalz, S., Downs, A.M., Vassy, J., Rigaut, J.P., 1991. Modelling and analysis of 3-D arrangements of particles by point process with examples of application to biological data obtained by confocal scanning light microscopy. J. Microsc. 161, 405–433.
Leblond, J.-B., Perrin, G., 1999. A self-consistent approach to coalescence of cavities in inhomogeneously voided ductile solids. J. Mech. Phys. Solids 47, 1823–1841.
Lee, J.A., Mykkanen, D.L., 1987. Metal and Polymer Matrix Composites. Noyes Data Corporation, NY.
Lee, H.K., Simunovic, S., 2000. A damage constitutive model of progressive debonding in aligned discontinuous fiber composites. Int. J. Solids Struct. 38, 875–895.
Lotwick, H.W., 1982. Simulations on some spatial hard core models, and the complete packing problem. J. Statist. Comput. Simul. 15, 295–314.
Louis, P., Gokhale, A.M., 1994. Application of image analysis for characterization of spatial arrangements of features in microstructure. Metall. Mater. Trans. A 26, 1449–1456.
Lu, G.Q., Ti, L.B., Ishizaki, K., 1994. A new algorithm for simulating the random packing of monosized powder in CIP processes. Mater. Manuf. Processes 9, 601–621.
Lubachevsky, B.D., Stillinger, F.H., 1990. Geometric properties of random disk packing. J. Stat. Phys. 60, 561–583.
Lubachevsky, B.D., Stillinger, F.H., Pinson, E.N., 1991. Disks vs spheres: contrasting properties of random packing. J. Stat. Phys. 64, 501–524.
Markov, K.Z., Willis, J.R., 1998. On the two-point correlation function for dispersions of nonoverlapping spheres. Math. Models Meth. Appl. Sci. 8, 359–377.
Murata, I., Mori, T., Nakagawa, M., 1996. Continuous energy Monte Carlo calculations of randomly distributed spherical fuels in high-temperature gas-cooled reactor based on a statistical geometry model. Nucl. Sci. Eng. 123, 96–109.
Nolan, G.T., Kavanagh, P.E., 1992. Computer simulation of random packing of hard spheres. Powder Technol. 72, 149–155.
Ogen, L., Troadec, J.P., Gervois, A., Medvedev, N., 1998. Computer simulation and tessellations of granular materials. In: Rivier, N., Sadoc, J.F. (Eds.), Foarms and Emulsions. Kluver, Dordrecht, pp. 527–545.
Okabe, A., Boots, B., Sugihara, K., 1992. Spatial Tessellations. Willey, NY.
Pyrz, R., 1994. Quantitative description of the microstructure of composites. Part I: Morphology of unidirectional composite systems. Compos. Sci. Technol. 50, 197–208.
Pyrz, R., Bochenek, B., 1998. Topological disorder of microstructure and its relation to the stress field. Imt. J. Solids Struct. 35, 2413–2427.
Quintanilla, J., Torquato, S., 1997. Microstructure functions for a model of statistically inhomogeneous random media. Phys. Rev. E 55, 1558–1565.
Rankenburg, I.C., Zieve, R.J., 2001. Influence of shape on ordering of granular systems in two dimensions. Phys. Rev. E 63, 61303-1–61303-9.
Reiter, T., Dvorak, G.J., Tvergard, V., 1997. Micromechanical models for graded composite materials. J. Mech. Phys. Solids 45, 1281–1302.
Ripley, B.D., 1977. Modeling spatial patterns. J. Roy. Statist. Soc. B 39, 172–212.
Ripley, B.D., 1981. Spatial Statistic. John Willey & Sons, NY.
Shan, Z., Gokhale, A.M., 2002. Representative volume element for non-uniform micro-structure. Comput. Mater. Sci. 24, 361–379.
Shubin, A.B., 1995. On maximum density of random packing of the identical solid spheres. Rasplavy N1, 92–97, in Russian.
Sinelnikov, N.N., Mazo, M.A., Berlin, A.A., 1997. Dense packing of random binary assemblies of disks. J. Phys. I France 7, 247–254.
Spowart, J.E., Maruyama, B., Miracle, D.B., 2001. Multi-scale characterization of spatially heterogeneous system: implication for discontinuously reinforced metal-matrix composite microstructures. Mater. Sci. Eng. A 301, 51–61.

Stoyan, D., 2000. Basic ideas of spatial statistics. In: Mecke, K.R., Stoyan, D. (Eds.), Statistical Physics and Spatial Statistics: the Art of Analyzing and Modeling Saptial Structures and Patern Formation. Lecture Notes in Physics, vol. 554, Berlin.

Stoyan, D., Kendall, W.S., Mecke, J., 1995. Stochastic Geometry and its Applications. J. Wiley & Sons, Chichester.

Stoyan, D., Stoyan, H., 1994. Fractals, Random Shapes and Point Fields. Methods og Geometric Statistics. J. Wiley & Sons, Chichester.

Suresh, S., Mortensen, A., 1998. Fundamentals of functionally graded materials : processing and thermomechanical behaviour of graded metals and metal-ceramic composites. IOM Communications Ltd., London.

Tandon, G.P., Kim, R.Y., Bechel, V.T., 2002. Construction of the fiber-matrix interface failure envelope in a polymer matrix composite. J. Multiscale Comput. Eng., submitted for publication.

Tanemura, M., 1979. On random complete packing by discs. Ann. Inst. Statist. Math. 31, 351–365.

Tobochnik, J., Chapin, P.M., 1988. Monte Carlo simulation of hard spheres near random closest packing using sphrical boundary conditions. J. Chem. Phys. 88, 5824–5830.

Torquato, S., 1997. Effective stiffness tensor of composite media: I. Exact series expansions.. J. Mech. Phys. Solids 45, 1421–1448.

Torquato, S., 1998. Effective stiffness tensor of composite media: II. Application to isotropic dispersions. J. Mech. Phys. Solids 45, 1421–1448.

Torquato, S., 2002. Random Heterogeneous Materials: Microstucture and Macroscopic Properties. Springer-Verlag, Berlin.

Torquato, S., Lado, F., 1992. Improved bounds on the effective elastic moduli of random arrays of cylinders. ASME. J. Appl. Mech. 59, 1–6.

Torquato, Stell, G., 1985. Microstructure of two-phase random media. J. Chem. Phys. 82, 980–987.

Torquato, S., Truskett, T.M., Debenetti, P.G., 2000. Is random close packing of spheres well defined? Phys. Rev. Letter 84, 2064–2067.

Turnbull, D., Cormia, R.L., 1960. A dynamic hard sphere model. J. Appl. Phys. 31, 674–678.

Widom, W., 1966. Random sequential addition of hard spheres to a volume. J. Chem. Phys. 44, 3888–3894.

Zinchenko, A.Z., 1994. Algorithm for random close packing of spheres with periodic boundary conditions. J. Comput. Phys. 114, 298–307.